Synthesis and characterization of $MoSe_2$ doped Co nanoparticles for advanced photocatalytic activity using MB dye

S. Bagyalakshmi[a], R. Uthrakumar[a,*], S. Aravindan[b], K. Parasuraman[c], K. Kaviyarasu[d]

[a]*Department of Physics, Govt. Arts College (Autonomous), Salem - 636007, Tamil Nadu, India*

[b]*Department of Physics, Chikkanna Government Arts College, Tirupur - 641602, Tamil Nadu, India*

[c]*Department of Physics, Sathyabama Institute of Science and Technology, Chennai-600 119, India*

[d]*UNESCO-UNISA Africa Chair in Nanosciences/Nanotechnology Laboratories, College of Graduate Studies, University of South Africa (UNISA), Muckleneuk Ridge, PO Box 392, Pretoria, South Africa*

$MoSe_2$-infused the sol-gel process was used to create Co nanoparticles, which will aid in photocatalytic degradation. Reducing the usage of hazardous chemicals and creating a green, ecologically friendly process for the production of both pure and doped MoSe2 nanoparticles were the primary goals of this effort. Furthermore, the impact of co-doping on photocatalysis activity was noted. Using transmission electron microscopy (TEM) analysis, ultraviolet–visible spectroscopy, the manufactured particles were examined using X-ray diffraction (XRD) and Fourier transform infrared spectroscopy (FTIR) was thoroughly characterized. About 93% of the methylene blue dye was removed from the doped samples after 150 minutes, indicating a considerable increase in photocatalytic activity.

(Received August 14, 2024; Accepted November 6, 2024)

Keywords $MoSe_2$ nanoparticles, Organic dye, UV-Visible, Photocatalytic performance, Transmission electron microscopy, Advanced oxidation process

1. Introduction

Because of their many technological uses in water treatment, photocatalysis, solar cells, photodetectors, computers, and optics, antimicrobial agents, other fields, metal oxide nanoparticles, often known as NPs, have garnered significant interest in academic and commercial research. These nanoparticles' direct binding energy of the excitation and large band gap pique the interest of most individuals. Molybdenum diselenide ($MoSe_2$) nanoparticles are made using a variety of physical and chemical techniques in conventional approaches. The physical techniques include sputtering, pulsed laser deposition, and evaporation [1–7]. It is also feasible to use chemical processes including pyrolysis, hydrolysis, sol-gel, solvothermal, and precipitation. These techniques produce trash that is harmful to the environment, require the use of hazardous chemicals, and require a lot of effort. The green synthesis method is a new sustainable approach that scientists and engineers are attempting to develop materials that get around these basic limitations of the physical and chemical approaches. This process makes it possible to produce NPs more quickly, cheaply, environmentally friendly, and non-toxicly. Green chemistry is fast developing topics of study that can assist generate targeted NPs in an environmentally responsible and reliable manner [8–15]. This is due to the fact that Co doping has the ability to create oxygen vacancies, which $MoSe_2$ can utilize as a surface site for water dissociation. Additionally, it can significantly raise electron-hole separation efficiency. Nonetheless, superoxide radical anions

*Corresponding author: uthraloyola@yahoo.com
https://doi.org/10.15251/DJNB.2024.194.1701

(*O_2−) can be produced by electrons trapped at the Co site during the oxidation process, as can the adsorbed O_2, and hydroxyl radical (*OH) can be produced by the holes reacting with the enclosed H2O [16–18]. Additionally, it has significant concentrations of citric and ascorbic acids, which serve as stabilizers and capping agents [19–22].

Recently, $MoSe_2$ NPs' photocatalytic properties have garnered a lot of interest for a variety of applications. One of them is the treatment of waste water. In this process, the electrons in the NPs absorb photonic energy and go to the conduction band from the valence band, where they form an electron-hole pair. These charge carriers break down organic contaminants into water and CO_2 and produce reactive free radicals like O_2* and OH*. Because of the $MoSe_2$ NPs' low band gap energy, electrons can move from the easily transitions from valence to the conduction band when photonic light is present. When this happens, hydroxyl radicals (OH*) may be produced by the combination of electrons with water molecules (H_2O). There is excellent photocatalytic activity in these free radicals [23–26]. The metal oxides have demonstrated that varying concentrations of cobalt have an impact on the size and structure of the particles. This has a discernible impact on methylene blue's (MB) photodegradation. After 150 minutes of UV light exposure, the bulk of the $MoSe_2$ NPs synthesized with Co doping showed good size and shape distribution and destroyed around 93% of the MB.

This study examines the enhanced photocatalytic activity of $MoSe_2$-doped Co NPs and their synthesis by a straightforward sol-gel method. The sample was analyzed using transmission electron microscopy (TEM), X-ray diffraction (XRD), ultraviolet-visible spectroscopy (UV-Vis), and Fourier transform infrared spectroscopy (FTIR). In order to determine the photodegradation rate and ensure their potential for usage in future photocatalysis applications, additionally, the NPs' photocatalytic activity on Methylene Blue (MB) has been examined.

2. Experimental

Using the sol-gel technique, $MoSe_2$ nanoparticles were created. Typically, 0.5 g of molybdenum (V) chloride ($MoCl_5$) and 1.14 g of diphenyl diselenide ($C_{12}H_{10}Se_2$, DDS) are mixed together in a beaker. 30 mL of excess ethanol was gradually added to the beaker and shaken with an ultrasonicator for 0.5 hours to obtain a homogenous solution before the mixture was dissolved in the ethanol under a fume hood. The gel-like precursor powders were prepared, allowed to dry, and then baked within a ceramic boat using a hot air oven. The residue is dried and then sintered in a muffle furnace for seven hours at 600°C. Using XRD, through transmission electron microscopy (TEM), FTIR, and UV-vis, the samples were found to meet the structural, morphological, and optical requirements for structural, morphological, and optical study.

3. Results and discussion

3.1. XRD analysis

Figure 1 shows the XRD graphs of both clean and doped $MoSe_2$ nanoparticles. The diffraction peaks at diffraction lines (101), (009), (107), (018), (110), (116), and 31.748°, 41.40°, 42.25°, 45.50°, 53.55°, 62.82°, and 66.33°, correspond to the reference number 75-0610 of the International Centre for Diffraction Data.The diffraction peaks are indicated by the XRD pattern has a space group of $P6_3/mmc$ and correlate to the hexagonal structure. The equivalent strong peaks (107 and 018) are visible among the nine notable peaks (101). The XRD pattern of Co does not exhibit any noticeable peaks, suggesting that Co can partially replace $MoSe_2$ without altering the crystal structure. Calculations are made for the micro-strain, lattice parameters, and average crystallite size. To compute these parameters, the following Williamson-Hall and Scherrer formulas are applied. The Scherrer and Williamson-Hall equations are given in Eq. (1) and Eq. (2) respectively.

$$D = k\lambda/\beta \cos\theta \quad (1)$$

$$\beta \cos \theta = k\lambda/D + 4\varepsilon \sin \theta \quad (2)$$

for both equations, go here,
D = Crystallite size average in nanometers
λ = Cu X-ray wavelength = 0.15406 nm.
K = 0.9 for the crystallite form factor
β = Complete width in radians at half maximan
θ = Bragg's angle in radians (θ)
ε = Micro-strain.

In terms of measuring methodology, the Scherrer equation and the Williamson-Hall charting both follow the trend. This could happen because of the more consistent interior arrangement of the particles. The refined data made the lattice parameter clear. This could happen if the lattice parameters drop or if Co nanoparticles are replaced.

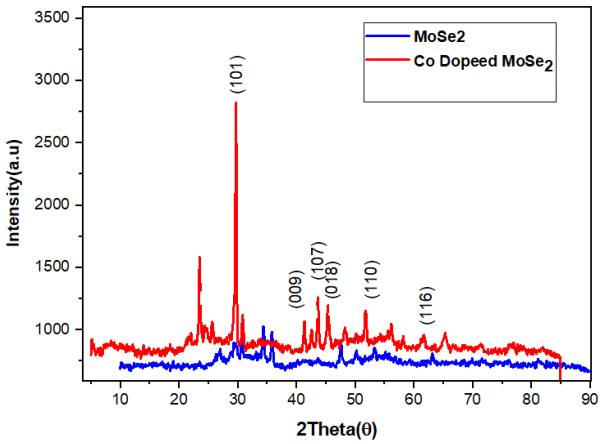

Fig. 1. XRD patterns of doped Co NPs and pure $MoSe_2$

3.2. UV-vis spectra studies

Figure 2 shows the UV–Vis absorption measurement of the synthesized $MoSe_2$ doped Co nanoparticles, which is examined at room temperature using UV–Vis Spectroscopy. It has been shown that absorbance first reduces sharply as wavelength increases. Following that, the absorbance coefficient value stays rather consistent, indicating that the synthesized particles have uniform sizes. The spectra under investigation showed a prominent peak of absorption at 325 nm. Figure 2 displays the results of the $MoSe_2$ nanoparticles' UV-vis absorption studies. Tauc relations can be used to derive the energy band gap (Eg) from the optical absorption spectra.

$$\alpha hv = A(hv - Eg)n \quad (3)$$

The constants that govern the kind of optical transitions are the band gap (Eg) and the absorbance coefficient (an) for both indirect (n = 2 and 3) and direct (n = 1/2 and 3/2, respectively) allowed and forbidden transitions.

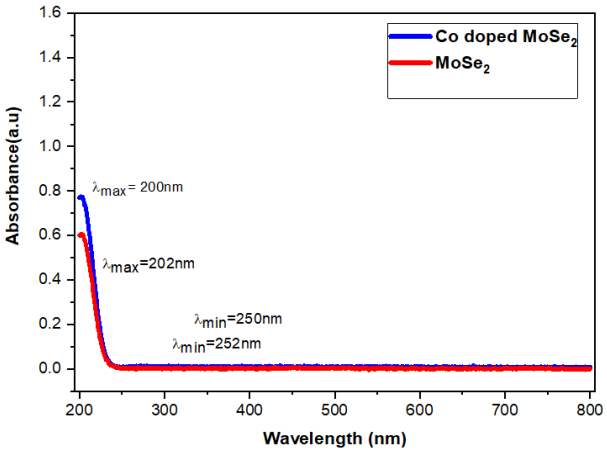

Fig. 2. UV-vis spectrum of pure and doped $MoSe_2$ NPs.

3.3. FTIR spectral analysis

Thermo Nicolet Avtar 370 model was used to record the FTIR spectra of $MoSe_2$ nanoparticles and $MoSe_2$-doped Co nanoparticles. The vibrational peak at 3642.79 cm^{-1} exhibits N-H stretching, which could be brought on by the presence of hydrazine hydrate. Our sample was synthesised in an aqueous solution, which led to the O-H stretching vibrational peak at 2430.07 cm^{-1}. Furthermore, the vibrational peak at 1384.43 cm^{-1}, which could be the outcome of ethylene glycol and hydrazine hydrate interacting, is caused by C-N stretching. The Mo-Se interaction is responsible for the vibrational peak observed in $MoSe_2$-doped Co at 830.87 cm^{-1}, while the H-OH stretching is indicated by the vibrational peak at 1051.01 cm^{-1}. The MoSe2 doped Co nanoparticles and pure $MoSe_2$ nanoparticles' FTIR spectra are shown in.

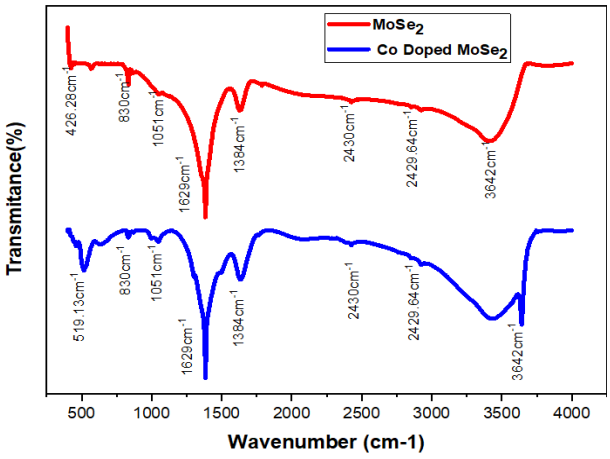

Fig. 3. FT-IR spectrum of pure and doped $MoSe_2$ NPs.

3.4. TEM studies

The morphology of the as-synthesised nanoparticles was investigated using a TEM Jeol Model JEM 2100. TEM was used to examine the size and morphology of the artificially generated $MoSe_2$ doped Co and $MoSe_2$ undoped Co nanoparticles. It also confirms the nanocrystallinity of the sample. It was also evident from the photo that there were several particles. The mean diameters of the doped Co and $MoSe_2$ nanoparticles were around 49 and 51 nm, respectively. This suggests that the kinetics of coarsening of the $MoSe_2$ nanoparticles were markedly enhanced by the Mg addition. Figure 4(a-c) displays the selected area electron diffraction (SAED) patterns and transmission electron microscopy (TEM) images of the MoSe2-doped and pure Co nanoparticles.

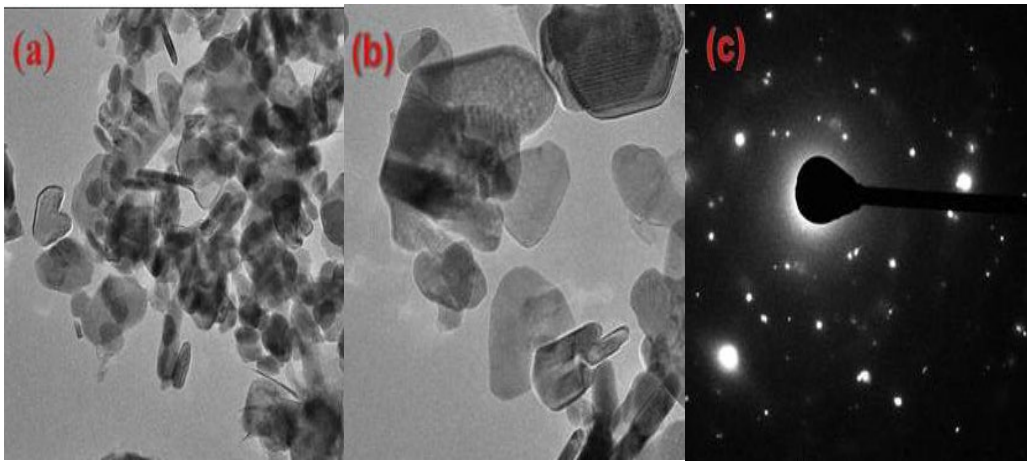

Fig. 4. TEM micrograph of $MoSe_2$with SAED pattern of pure and doped $MoSe_2$ NPs.

3.5. Photocatalytic analysis

The methylene blue (MB) dye's UV–Vis absorption spectrum at various intervals following the addition of pure, doped $MoSe_2$ nanoparticles are displayed in Figure 5(a&b). The wavelength at which the absorbance is maximum, according to the absorption spectra, is 665 nm. The absorbance gradually drops once the photocatalyst is added, showing that the particles can carry out a reaction of dye degradation driven by light.

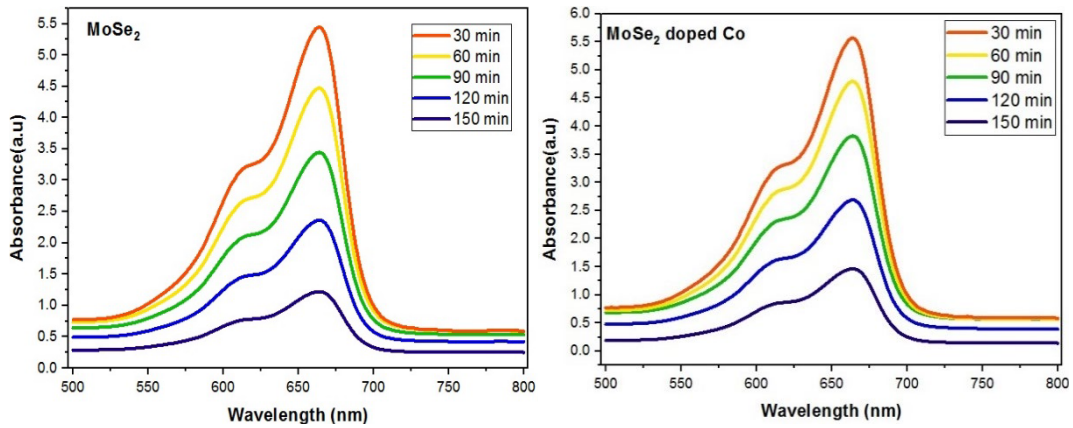

Fig. 5. (a) UV-vis spectra during photocatalytic treatment of MB under UV-light irradiation of pure $MoSe_2$ NPs; (b) UV-vis spectra during photocatalytic treatment of MB under UV-light irradiation of doped $MoSe_2$ NPs.

The rate of degradation for every photocatalyst is shown in Figure 6. Pure $MoSe_2$ nanoparticles show the least deterioration compared to the other samples because of their greater band gap. The effectiveness of the Co-doped $MoSe_2$ nanoparticles is still inferior to that of the other doping concentrations, despite their superior performance over the pure ones. This behavior could be brought on by dopants being present in sufficient concentration. It's possible that improper doping was done because of the low dopant concentration. The formula is used to calculate the percentage of absorption of each drug [27-29].

$$D(\%) = \frac{C_0 - C_t}{C_0} \times 100 \quad (5)$$

where C_0 and Ct stand for the beginning and terminal concentrations, respectively. Consequently, the rate of degradation stays rather close to the pure sample. However, both the pure and co-doped $MoSe_2$ nanoparticles exhibit remarkable performance in C/C_0, as shown in Fig. 7(a-b). They degrade at a very rapid rate in comparison to other samples.

Possible explanations include the presence of dopants that replaced the Co ions in the $MoSe_2$ lattice. As a result, the particles get smaller, which increases their surface area and promotes the dye's adhesion. An additional explanation could be the cooperative effect of Co doping in $MoSe_2$ nanoparticles. Doping increases the reactivity of the photocatalysts by significantly narrowing the band gap. The photocatalyst can absorb a greater variety of light wavelengths due to its narrower bandgap. Consequently, photocatalyst increases visible light absorption, which is necessary for practical applications.

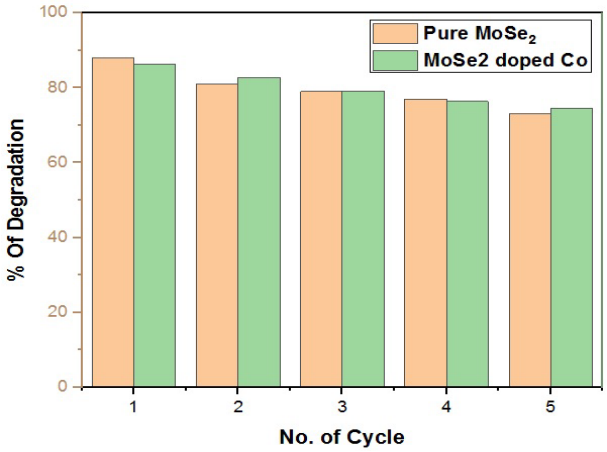

Fig. 6. Recycle efficiency of MB on $MoSe_2$ doped Co nanoparticles.

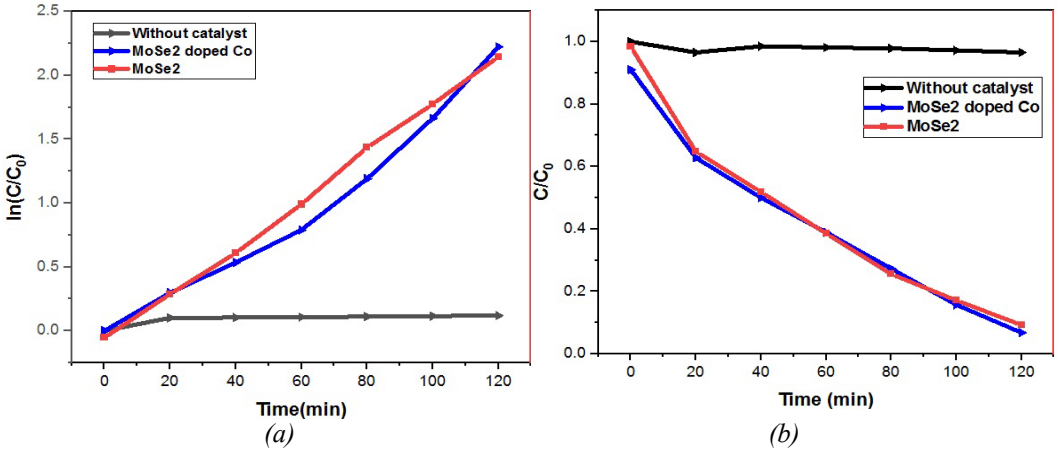

(a) *(b)*

Fig. 7 (a). Degradation efficiency plot MB's irradiation time against C/Co on $MoSe_2$ doped Co NPs; Plot of MB irradiation period versus degradation efficiency C/Co on $MoSe_2$ doped Co NPs.

A notable reduction in the dependence the photocatalytic activity rises in response to UV light. Furthermore, a smaller bandgap encourages the production of charge carriers. Through their interactions with the dye, these charge carriers quicken the degradation process. The following illustrates the processes linked to photocatalytic activity-induced dye degradation.

The degradation process could be represented by the following equations

$$MoSe_2 + hv \rightarrow Co\ (e^-_{CB} + h^+_{VB}) \quad (4)$$

$h^{+}_{VB} + MB \rightarrow MB^{+} \rightarrow$ oxidation of MB, (5)

$h^{+}_{VB} + H_2O(OH^{-}) \rightarrow OH^{*} + H^{+}$ (6)

$OH^{*} + MB\ dye \rightarrow CO_2 + H_2O.$ (7)

Charge carrier recombination is a drawback of a narrower bandgap. The photocatalytic mechanism of MB dye, which employs a catalyst in the presence of visible light, is demonstrated in Figure 8. Nevertheless, the efficient doping of Co ions into the $MoSe_2$ lattice sinks the electrons. As thus, the decrease in electron-hole pair recombination increases the activity of photocatalysis.

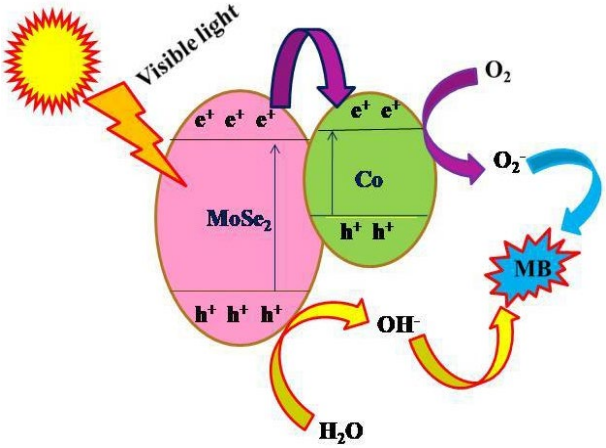

Fig. 8. Diagram showing the photocatalytic process of MB dye utilizing a catalyst in the presence of light.

4. Conclusion

In conclusion, the ability of nanomaterials to efficiently utilize organic waste and eliminate non-toxic contaminants has led to their increasing significance in this quickly evolving era of science and technology. This article provided instructions for making $MoSe_2$ nanoparticles using the sol-gel process in a quick and affordable manner. By adjusting their concentration, the doping components' effect may be seen. The photocatalytic activity of $MoSe_2$ nanoparticles, both doped and undoped, was examined. The XRD measurements showed that the nanoparticles were arranged in a hexagonal pattern. Stretching vibration will happen at higher doping percentages, according to the FTIR data. TEM analysis reveals the size of the NPs and the presence of chemical components in the produced NPs, and these findings are consistent with the updated XRD 51.57 nm and 49.09 nm, respectively, the diameters of the pure and doped samples for Co-doped and pure NPs.

The UV-Vis data indicates that, in comparison to doped nanoparticles, doped samples generate a progressive reduction in the band gap. Doped nanoparticles had an extraordinary photodegradation rate in comparison to undoped ones; 150 minutes later, the degradation rate for Co-doped NPs was strikingly near to 93%. Therefore, when synthesised $MoSe_2$ nanoparticles and co-doped $MoSe_2$ with remarkable photodegradation properties are used, the study's results imply that reducing agents that are natural, renewable, and harmless for the environment the prepared nanoparticles can be used for photocatalytic applications.

References

[1] M.J. Muño, D. Bahnemann, Sol. Energy. 77, (2004) 445-459;
https://doi.org/10.1016/j.solener.2004.03.031

[2] B. Chen, Y. Meng, J. Sha, C. Zhong, W. Hu, N. Zhao, Nanoscale. 10, (2017) 34-68;

https://doi.org/10.1039/C7NR07366F

[3] B.J. Rani, G. Ravi, R. Yuvakkumar, S. Ravichandran, F. Ameen, A. Al-Sabri, 89 (2018) 500-510; https://doi.org/10.1007/s10971-018-4886-5

[4] E. T. Selvi, R Uthrakumar, C Inmozhi, K Kaviyarasu, Digest Journal of Nanomaterials & Biostructures (DJNB) 19 (2024) p. 115, https://doi.org/10.15251/DJNB.2024.191.115

[5] S Bagyalakshmi, M Subash, R Uthrakumar, S Aravindan, K Kaviyarasu, Digest Journal of Nanomaterials & Biostructures (DJNB) 19 (2024) p.201 , https://doi.org/10.15251/DJNB.2024.191.201

[6] R.A.C. Amoresi, R.C. Oliveira, N.L. Marana, P.B. De Almeida, P.S. Prata, M.A. Zaghete, E. Longo, J.R. Sambrano, A.Z. Simões, ACS Appl. Nano Mater. 2 (2019) 6513-6526; https://doi.org/10.1021/acsanm.9b01452

[7] C.N.C. Hitam, A.A. Jalil, J. Environ. Manage. 258 (2020) 110050; https://doi.org/10.1016/j.jenvman.2019.110050

[8] K. Kaviyarasu, P.A. Devarajan, S.S.J. Xavier, S.A. Thomas, S. Selvakumar, Journal of Materials Science & Technology 28 (1), (2012), 15-20; https://doi.org/10.1016/S1005-0302(12)60017-6

[9] V. Perumal, C. Inmozhi, R. Uthrakumar, R. Robert, M. Chandrasekar, S. Beer Mohamed, Shehla Honey, A. Raja, Fahd A. Al-Mekhlafi, K. Kaviyarasu, Environmental Research, 209, (2022), 112821; https://doi.org/10.1016/j.envres.2022.112821

[10] K. Kasinathan, J. Kennedy, M. Elayaperumal, M. Henini, M. Malik, Scientific reports 6 (1), 1-12, 2016; https://doi.org/10.1038/srep38064

[11] R. M. Surya, S. Mauliddiyah, D. O.B. Apriandanu, Sudirman, Y. Yulizar, Chemosphere, 304 (2022)135125; https://doi.org/10.1016/j.chemosphere.2022.135125

[12] J. Al Boukhari, L. Zeidan, A. Khalaf, R. Awad, Chem. Phys. 516 (2019) 116-124; https://doi.org/10.1016/j.chemphys.2018.07.046

[13] S. Agrawal, A. Parveen, A. Azam, J. Lumin. 184 (2017) 250-255; https://doi.org/10.1016/j.jlumin.2016.12.035

[14] H. Abbas, K. Nadeem, H. Krenn, M. Kostylev, J. Hester, A.T. Murdock, S. Yick, I. Letofsky-Papst, C. Ulrich, Nanotechnology. 31 (2020) 475701; https://doi.org/10.1088/1361-6528/abaf23

[15] M. Chandrasekar, S. Panimalar, R. Uthrakumar, M. Kumar, M.E. Raja Saravanan, G. Gobi P. Madheswaran, C. Inmozhi, K. Kaviyarasu, Materials Today: Proceedings, 36, (2021), 228-231; https://doi.org/10.1016/j.matpr.2020.03.228

[16] M.V. Arularasu, M. Anbarasu, S. Poovaragan, R. Sundaram, K. Kanimozhi, C. Maria Magdalane, K. Kaviyarasu, F.T. Thema, Douglas Letsholathebe, Genene T. Mola, M. Maaza, Journal of nanoscience and nanotechnology 18 (5), (2018), 3511-3517; https://doi.org/10.1166/jnn.2018.14658

[17] S. Panimalar, R. Uthrakumar, E. Tamil Selvi, P. Gomathy, C. Inmozhi, K. Kaviyarasu, J. Kennedy, Surfaces and Interfaces 20, (2020) 100512; https://doi.org/10.1016/j.surfin.2020.100512

[18] Amal George, D. MagimaiAntoni Raj, X. Venci, A. Dhayal Raj, A. Albert Irudayaraj, R.L. Josephine, S. John Sundaram, Amal A. Al-Mohaimeed, Dunia A. Al Farraj, Tse-Wei Chen, K. Kaviyarasu, Environmental Research, 203, (2022) 111880; https://doi.org/10.1016/j.envres.2021.111880

[19] L.S. Nair, D. Chandran, V.M. Anandakumar, K. R. Babu, Ceram. Int. 43 (2017) 11090-11096; https://doi.org/10.1016/j.ceramint.2017.05.155

[20] K.V. Chandekar, Mohd. Shkir, A. Khan, M.A. Sayed, N. Alotaibi, T. Alshahrani, H. Algarni, S. AlFaify, J. Mater. Res. Technol. 15, (2021) 2584-2600; https://doi.org/10.1016/j.jmrt.2021.09.072

[21] G. Bharathy, P. Raji, J. Mater. Sci. Mater. Electron. 28, (2017) 17889-17895; https://doi.org/10.1007/s10854-017-7730-8

[22] K.N. Patel, M.P. Deshpande, K. Chauhan, P. Rajput, V.P. Gujarati, S. Pandya, V. Sathe, S.H.Chaki, Adv. Powder Technol. 29, (2018) 2394-2403; https://doi.org/10.1016/j.apt.2018.06.018

[23] S. Panimalar, S. Logambal, R. Thambidurai, C. Inmozhi, R. Uthrakumar, AzhaguchamyMuthukumaran, Rabab Ahmed Rasheed, Mansour K. Gatasheh, A. Raja, J. Kennedy, K. Kaviyarasu, Environmental Research, 205, (2022) 112560; https://doi.org/10.1016/j.envres.2021.112560

[24] A. Raja, K. Selvakumar, P. Rajasekaran, M. Arunpandian, S. Ashokkumar, K. Kaviyarasu, S. Asath Bahadur, M. Swaminathan, Colloids and Surfaces A: Physicochemical and Engineering Aspects, 564, (2019), 23-30; https://doi.org/10.1016/j.colsurfa.2018.12.024

[25] V. Perumal, A. Sabarinathan, M. Chandrasekar, M. Subash, C. Inmozhi, R. Uthrakumar, Abdulgalim B. Isaev, A. Raja, Mohamed S. Elshikh, SaeedahMusaed Almutairi, K. Kaviyarasu, Fuel, 324, (2022), 124599; https://doi.org/10.1016/j.fuel.2022.124599

[26] S. Panimalar, M. Chandrasekar. S. Logambal, R. Uthrakumar, C. Inmozhi, Materials Today: Proceedings, 56, (2022), 3394-3401; https://doi.org/10.1016/j.matpr.2021.10.335

[27] M. Chandrasekar, M. Subash, V. Perumal, S. Panimalar, S. Aravindan, R. Uthrakumar, C. Inmozhi, Abdulgalim B. Isaev, Sudhakar Muniyasamy, A. Raja, K. Kaviyarasu, Separation and Purification Technology, 294, (2022), 121189; https://doi.org/10.1016/j.seppur.2022.121189

[28] M. Chandrasekar, M. Subash, S. Logambal, G. Udhayakumar, R. Uthrakumar, C. Inmozhi, Wedad A. Al-Onazi, Amal M. Al-Mohaimeed, Tse-Wei Chen, K. Kanimozhi, J. King Saud Uni. - Sci., 34, (2022), 101831; https://doi.org/10.1016/j.jksus.2022.101831

[29] R. Abinaya, J. Archana, S. Harish, M. Navaneethan, S. Ponnusamy, C. Muthamizhchelvan, M. Shimomura, and Y. Hayakawa, RSC Adv. 8, (2018), 26664; https://doi.org/10.1039/C8RA02560F